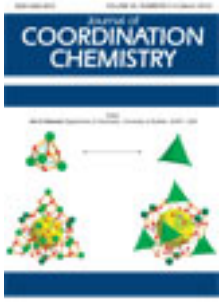

Journal of Coordination Chemistry
Publication details, including instructions for authors and subscription information:
http://www.tandfonline.com/loi/gcoo20

Synthesis and characterization of self-assembled coordination polymers of N-diaminomethylene-4-(3-formyl-4-hydroxy-phenylazo)-benzenesulfonamide

Hoda El-Ghamry [a], Ken Sakai [b], Shigeyuki Masaoka [c], Kamal El-Baradie [a] & Raafat Issa [a]

[a] Chemistry Department, Faculty of Science, Tanta University, Tanta, Egypt

[b] Chemistry Department, Faculty of Science, Kyushu University, Fukuoka, Japan

[c] Institute for Molecular Science, Higashiyama 5-1, Myodaiji, Okazaki 444-8787, Japan

Published online: 15 Feb 2012.

To cite this article: Hoda El-Ghamry, Ken Sakai, Shigeyuki Masaoka, Kamal El-Baradie & Raafat Issa (2012) Synthesis and characterization of self-assembled coordination polymers of N-diaminomethylene-4-(3-formyl-4-hydroxy-phenylazo)-benzenesulfonamide, Journal of Coordination Chemistry, 65:5, 780-794, DOI: 10.1080/00958972.2012.661418

To link to this article: http://dx.doi.org/10.1080/00958972.2012.661418

Journal of Coordination Chemistry
Vol. 65, No. 5, 10 March 2012, 780–794

Synthesis and characterization of self-assembled coordination polymers of *N*-diaminomethylene-4-(3-formyl-4-hydroxy-phenylazo)-benzenesulfonamide

HODA EL-GHAMRY*†, KEN SAKAI‡, SHIGEYUKI MASAOKA§, KAMAL EL-BARADIE† and RAAFAT ISSA†

†Chemistry Department, Faculty of Science, Tanta University, Tanta, Egypt
‡Chemistry Department, Faculty of Science, Kyushu University, Fukuoka, Japan
§Institute for Molecular Science, Higashiyama 5-1, Myodaiji, Okazaki 444-8787, Japan

(*Received 24 September 2011; in final form 21 November 2011*)

The azo dye ligand *N*-diaminomethylene-4-(3-formyl-4-hydroxy-phenylazo)-benzenesulfonamide (HL) and Cu(II), Co(II), and Mn(II) coordination polymers were synthesized in addition to a non-polymeric Pd(II) complex. In all complexes, the ligand bonds to the metal ion through the formyl and α-hydroxy oxygen atoms. The sulfonamide oxygen also coordinates to the metal. The complexes are formulated as $[ML_2]_n$, where M = Cu(II), Co(II), and Mn(II), and $[ML(Cl)(H_2O)]$, where M = Pd(II). On the basis of spectral studies and magnetic susceptibility measurements, an octahedral geometry was assigned to Co(II) and Mn(II) complexes, tetragonally elongated octahedral geometry for Cu(II) complex, while the Pd(II) complex was found to be square planar. Crystallization of Cu(II) complex from DMF afforded single crystals of general formula $\{[Cu(L)_2] \cdot 3DMF\}_n$ (**2**). X-ray structural analysis of **2** revealed that each Cu(II) adopts elongated octahedral geometry affording 1-D chains. The chains are connected by hydrogen bonds, resulting in the formation of 2-D supramolecular assemblies. The crystal structure of HL has also been determined and discussed. Cyclic voltammetric behavior of the ligand and some complexes are also discussed.

Keywords: Sulfaguanidine; Coordination polymers; Metal complexes; Cyclic voltammetry; Crystal structure

1. Introduction

Attention has been paid to the design and synthesis of metal-organic frameworks [1] for applications in electrical conductivity [2], magnetism [3], host-guest chemistry [4], sensors [5], and catalysis [6]. The framework structures of coordination polymers primarily depend on coordination preferences of the central metal ions and the functionality of the ligands. Aside from bonding interactions, hydrogen bonding, and π–π stacking interactions, the solvent, counter ions, and the ratio of metal salt to organic ligand also influence the formation of the ultimate architectures [7].

*Corresponding author. Email: helghamrymo@yahoo.com

ISSN 0095-8972 print/ISSN 1029-0389 online
http://dx.doi.org/10.1080/00958972.2012.661418

Sulfa-drugs are widely used in the treatment of infections, especially for patients intolerant to antibiotics. The vast commercial success of these medical agents has made the chemistry of sulfonamides a major area of research and important in pharmaceutical sciences [8]. The sulfadrugs and their azo derivatives have applicability as potential ligands for a large number of metal ions [9–12]. A literature survey reveals supramolecular assembly of polymer complexes based on azo-derivatives of aliphatic and/or aromatic amine sulfa drugs [9–15]. The metal chelates thus produced have wide applications in the dye industry, as analytical reagents for micro-determination of metals and in biological applications [16]. Moreover, azo dyes derived from sulfonamides and their metal complexes have wide interest in application to electrochemical studies [17].

We report here the synthesis and characterization of a new sulfaguanidine azo dye, (HL), and supramolecular networks constructed by the ligand in combination with Cu(II), Co(II), and Mn(II). We also report the non-polymeric system using Pd(II). Cyclic voltammetric behavior of the ligand and some selected metal complexes were also studied.

2. Experimental

2.1. *Synthesis of the ligand*

HL was prepared by the coupling of sulfaguanidine diazonium salt with salicylaldehyde [18].

2.2. *Synthesis of metal complexes: general procedure*

Metal complexes were prepared by mixing appropriate amounts of the ligand in a MeOH/DMF mixture (50% V/V) with the hydrated metal chlorides [$CuCl_2 \cdot 2H_2O$, $CoCl_2 \cdot 6H_2O$, $MnCl_2 \cdot 4H_2O$, and K_2PdCl_4] in absolute methanol with molar ratio 2 L : 1 M or 1 L : 1 M in the presence of few drops of triethyl amine as basic medium. The resulting solutions were then refluxed with stirring for 4 h; the solid complexes were separated out while hot and were collected by filtration and dried.

2.3. *Materials and physical measurements*

Solvents and starting materials (sulfaguanidine and metal chlorides) were purchased from TCI and Wako chemical companies, Tokyo, and used as received. Elemental analysis was carried out on a Perkin Elmer 2400II CHN. ESI-TOF mass spectra (ESI-TOF MS) were recorded on a JEOL JMS-T100LC mass spectrometer. The measurements were performed in the negative ion mode at the cone voltage of −30 V. ^{1}H-NMR spectra were recorded on a JEOL JNM-AL300 spectrometer. UV-Visible absorption spectra were recorded on a Shimadzu UV-2450 spectrophotometer using nujol mulls. Infrared (IR) spectra were achieved using a Perkin-Elmer Spectrum One FT-IR spectrometer equipped with a single reflection diamond ATR accessory. X-band ESR spectra were recorded at 25°C on a JEOL model JM-FE3 spectrometer provided

by JEOL microwave unit using diphenylpicrylhydrazyl (DPPH) as the reference. The simulated X-ray powder diffraction (XRD) pattern based on single-crystal data was prepared using Mercury software [19]. X-ray diffraction analyses were carried out with a PW 1840 Philips diffractometer with Cu-Kα radiation ($\lambda = 1.542$). Thermogravimetric analyses (TGA and DTG) were performed on a Shimadzu TG-50 thermal analyzer in a dynamic nitrogen atmosphere with a heating rate of $10^{\circ}C\,min^{-1}$. Magnetic susceptibility measurements at room temperature (25°C) were determined on a Johnson Matthey magnetic susceptibility balance. Conductance measurements were carried out on a YSI model 32 conductance meter in DMF ($10^{-3}\,mol\,L^{-1}$). Cyclic voltammograms were obtained on an ALS-620S electrochemical analyzer under Ar atmosphere at 20°C using a three-electrode cell in which a platinum electrode was the working electrode, Ag/AgCl electrode was the reference electrode, and platinum wire was used as the auxiliary electrode. A ferrocene/ferrocenium couple was used as an internal standard; $E_{1/2}$ of the ferrocene/ferrocenium couple under the experimental conditions is 172 mV. Tetra (*n*-butyl) ammonium perchlorate (TBAP), $0.1\,mol\,L^{-1}$, was used as the supporting electrolyte.

2.4. *X-ray crystallography*

Single-crystals of HL were obtained by vapor diffusion of water through DMF solution of the ligand at room temperature, resulting in the formation of yellow needles; single crystals of **2** were obtained by crystallization of **1** from DMF by slow evaporation at room temperature. After 2 weeks, pale brown blocks of **2** were obtained. A single crystal suitable for X-ray crystallography of each compound was mounted on a glass fiber using paratone oil. Data were collected by a Bruker SMART APEX2/CCD-based diffractometer with monochromated Mo-Kα radiation ($\lambda = 0.710373$ Å) from a rotating anode source with mirror-focusing apparatus. Cell parameters were retrieved using APEX II software [20] and refined using SAINT [20] on all the observed reflections. Data reduction was performed using SAINT. Absorption corrections were applied using SADABS [21]. The structures were solved by direct methods using SHELXS-97 [22] and refined by least-squares on F^2 using SHELXL-97 and KENX [23] programs.

3. Results and discussion

3.1. *Mass spectroscopy*

The mass spectrum of HL shows molecular ion peak at m/z 346.06 corresponding to $[L]^-$ moiety, which is consistent with the proposed molecular formula of the ligand.

3.2. *^{1}H-NMR spectra*

^{1}H-NMR spectra of the ligand and the diamagnetic Pd(II) complex were recorded in d^6-DMSO using tetramethylsilane (TMS) as an internal standard. The spectrum of HL shows three resonances at 11.61, 10.38, and 8.2–7.2 which are assigned to the phenolic OH, CHO, and phenyl ring [24]. The broad signal which appears at 6.68 ppm integrated

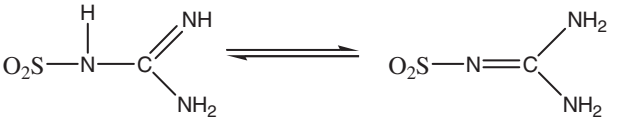

Scheme 1. Imino-amino tautomeric equilibrium in HL.

for the four protons of two NH_2 groups [25]. The appearance of such signal is favored through the tautomeric shift in the sulfonamide moiety shown in scheme 1.

In the spectrum of the Pd(II) complex, the signal characteristic for OH disappears, indicating coordination of the OH to the metal through deprotonation. The CHO signal shifts to lower frequencies (9.53) owing to complexation. The broad signal at 4.5 ppm is integrated to the coordinated water molecule. The signals characteristic for NH_2 and phenyl protons appeared at nearly the same positions as in the spectrum of the ligand.

3.3. *Molar conductivity measurements*

The molar conductance values of 10^{-3} mol L^{-1} solutions of the metal complexes were calculated at room temperature (table 1). The non-electrolytic nature of the metal complexes was confirmed by the low molar conductance values measured for DMF solution of the compounds [26] ($\Lambda_M = 6.1$–$20.5\ \Omega^{-1}\,cm^2\,mol^{-1}$).

3.4. *Crystal structure of HL*

The crystallographic and refinement data of HL and **2** are collected in table 2. X-ray structure analysis of HL indicated that crystals of HL are monoclinic with *P2(1)/c* space group. The X-ray structure of HL is shown in figure 1. The two aromatic groups attached to the azo double bond are *trans*. The guanidine consisting of C14 and N3–N5 together with both the central and terminal benzene rings exhibit a planar geometry (r.m.s deviations are 0.0028, 0.0064, and 0.0063 Å, respectively). The guanidinum is twisted with respect to the central phenyl ring at an angle of 79.83(15)° while the angle between the central and terminal benzene rings is 5.12(8)°. All bond lengths and angles are within the normal values [27] (table 3). Three intramolecular hydrogen bonds (N5–H10A···O3, O2–H5···O1, and N5–H10A···S1) stabilize the conformation of the molecule while two intermolecular hydrogen bonds (N4–H11B···O3(i) and N5–H10B···O1(ii); symmetry operation (i): $x+1$, $1.5-y$, $z+0.5$, (ii): $1-x$, $y-0.5$, $1.5-z$) stabilize the conformation together with the crystal packing (table 4).

3.5. *Crystal structure of 2*

Single-crystal X-ray analysis of **2** revealed that the complex crystallizes in triclinic lattice with *P-1* space group. The asymmetric unit contains one independent molecule of metal complex and three DMF molecules (figure 2). In **2**, the Cu(II) lies on a center of symmetry and has an elongated octahedral coordination geometry in which the two molecules of the bidentate ligand are *trans* with respect to each other, forming the equatorial plane. Each ligand coordinates to Cu(II) *via* formyl oxygen and

Table 1. Analytical and physical data of HL and metal complexes.

Compound No.	Formula	Color	F.W.	M.p.	Analysis found (calculated) (%)				Λ ($\Omega^{-1}mol^{-1}cm^2$)	μ_{eff} (B.M.)
					C	H	N	S		
HL	$C_{14}H_{13}N_5O_4S$	Orange	347	290[a]	48.20 (48.41)	3.86 (3.74)	19.97 (20.17)	9.02 (9.22)	–	–
1	$[CuL_2]$ $C_{28}H_{24}N_{10}O_8S_2Cu$	Greenish brown powder	756.2	>300	44.12 (44.47)	3.38 (3.20)	18.16 (18.52)	8.16 (8.46)	6.1	1.79
2	$[CuL_2]\cdot 3DMF$ $C_{37}H_{45}N_{13}O_{11}S_2Cu$	Pale brown crystals	975.25	>300	45.56 (45.29)	4.65 (4.49)	18.67 (18.54)	6.56 (6.31)	6.1	1.79
3	$[CoL_2]$ $C_{28}H_{24}N_{10}O_8S_2Co$	Orange yellow	751.6	>300	44.58 (44.74)	3.34 (3.22)	18.47 (18.64)	8.37 (8.15)	12.1	4.82
4	$[MnL_2]$ $C_{28}H_{24}N_{10}O_8S_2Mn$	Orange	747.6	>300	44.92 (44.98)	3.23 (3.24)	18.67 (18.74)	8.49 (8.56)	8.9	5.96
5	$[PdLCl(H_2O)]$ $C_{14}H_{14}N_5O_5SClPd$	Dark brown	505.9	>300	33.83 (33.22)	2.96 (2.79)	14.52 (13.83)	6.67 (6.32)	20.5	diam.

Table 2. Crystallographic data for HL and **2**.

	HL	**2**
Empirical formula	$C_{14}H_{13}N_5O_4S$	$C_{37}H_{45}N_{13}O_{11}S_2Cu$
Formula weight	347.35	975.52
Temperature (K)	100(2)	100(2)
Color, habit	Yellow, needles	Pale brown, blocks
Crystal system	Monoclinic	Triclinic
Space group	*P2(1)/c*	*P-1*
Unit cell dimensions (Å, °)		
a	6.8312(9)	7.007(15)
b	33.415(4)	12.156(3)
c	6.7046(9)	12.997(3)
α	90.00	91.874(2)
β	111.144(2)	104.253(2)
γ	90.00	91.676(2)
Volume (Å^3), *Z*	1427.4(3), 4	1071.7(4), 1
Calculated density (g cm^{-3})	1.616	1.511
Absorption coefficient (Mo-Kα) (mm^{-1})	0.26	0.68
F(000)	720	507
Crystal size (mm^3)	$0.2 \times 0.1 \times 0.1$	$0.2 \times 0.15 \times 0.1$
Radiation (Å)	0.71073	0.71073
θ range for data collection (°)	$25.02 < \theta < 2.44$	$25.4 < \theta < 1.62$
Index ranges	$-8 < h < 8$; $-39 < k < 39$; $-7 < l < 7$	$-8 < h < 7$; $-14 < k < 14$, $-15 < l < 15$
Reflections measured	13,242	7384
Unique reflections	2509	6033
Parameters refined	217	588
Goodness-of-fit on F^2	1.237	1.043
R(int)	0.035	0.018
R_1	0.0686	0.0401
wR_2	0.1511	0.1089
Largest difference peak and hole (e Å^{-3})	0.912 and −0.335	0.817 and −0.491

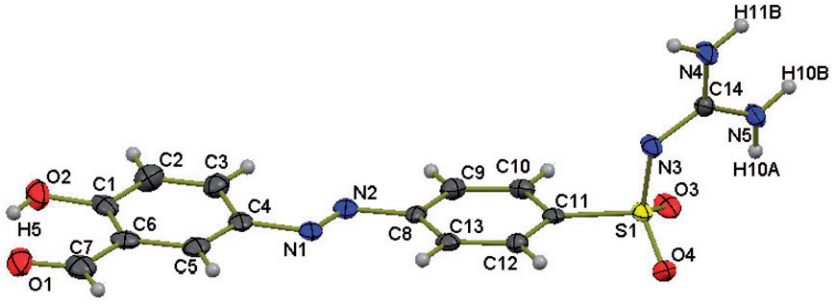

Figure 1. Molecular structure of HL showing the atom-labeling scheme. Displacement ellipsoids are drawn at the 50% probability level.

deprotonated α-hydroxy oxygen. The tetragonal structure is completed *via* coordination of Cu to sulfonamide oxygen atoms from neighboring molecules, resulting in the formation of an extended 1-D chain along the *b*-axis (figure 3). The Cu–O bond lengths [Cu1–O1 = 1.901(2) Å and Cu1–O2 = 1.967(2) Å] and O–Cu–O bond angles [O1–Cu1–O2 = 93.1(9)°, O1–Cu1–O1* = 180(1)°, O2–Cu1–O1* = 86.9(9)°; symmetry code (*)

Table 3. Selected bond lengths (Å) and angles (°) of HL and **2**.

HL		**2**	
S1–O4	1.438(3)	Cu1–O1	1.901(2)
S1–N3	1.589(3)	Cu1–O1*	1.901(2)
S1–C11	1.766(4)	Cu1–O2	1.966(2)
C1–O2	1.389(5)	Cu1–O4$^{\$}$	2.533(2)
N4–C14	1.331(5)	Cu1–O4$^{\#}$	2.533(2)
O1–C7	1.225(5)	S1–O3	1.434(2)
C4–C5	1.362(6)	S1–N3	1.580(3)
C8–N2	1.418(5)	O1–C1	1.285(4)
N2–N1	1.250(5)	N1–N2	1.247(4)
C6–C1–O2	122.3(4)	C4–C5	1.372(5)
N2–N1–C4	112.0(3)	N6–C16	1.456(5)
O4–S1–O3	115.09(18)	O1–Cu1–O1*	180.000(1)
O4–S1–N3	111.60(18)	O1–Cu1–O2	93.09(9)
N5–C14–N3	125.7(3)	O1–Cu1–O4$^{\$}$	88.42(8
C14–N3–S1	122.3(3)	O2–Cu1–O4$^{\#}$	97.63(8)
C10–C11–C12	121.0(4)	O3–S1–O4	116.77(14)
C13–C8–N2	125.5(4)	O3–S1–N3	106.20(15)
C3–C4–N1	122.2(4)	C1–O1–Cu1	126.6(2)
O1–C7–C6	121.6(5)	N1–N2–C8	116.6(3)

(*) $-x+3$, $-y+1$, $-z+1$; (\$) $-x+4$, $2-y$, $1-z$; (#) $x-1$, $y-1$, z.

Table 4. Hydrogen-bond geometries (Å, °) of HL and **2**.

D–H···A	D[a]–H	H···A[b]	D···A	D–H···A
HL				
N5–H10A···O3	0.88	2.19	2.804(4)	126.2
O5–H5···O1	0.84	1.92	2.633(5)	141.9
N5–H10A···S1	0.88	2.65	2.964(3)	102.6
N4–H11B···O3^{i}	0.88(7)	2.12(7)	2.943(4)	154.4(6)
N5–H10B···O1^{ii}	0.88(7)	1.98(7)	2.85(4)	170.4(6)
2				
N5–H5B···O4	0.88	2.14	2.787(11)	131.38
N4–H4B···N3^{iii}	0.88	2.09	2.95(11)	173.73
N4–H4A···O5^{iv}	0.88	2.02	2.79(4)	149.1
N5–H5A···O5^{iv}	0.88	2.1	2.85(4)	145.4

Symmetry codes: (i) $x+1$, $1.5-y$, $0.5+z$; (ii) $1-x$, $y-0.5$, $1.5-z$; (iii) $4-x$, $3-y$, $-z$; (iv) $3-x$, $2-y$, $-z$.
[a]Acceptor.
[b]Donor.

$-x+3$, $-y+1$, $-z+1$] are within the expected ranges [28]. The coordination bond distances in the axial direction, Cu1–O4$^{\&}$ and Cu1–O4$^{\#}$, are longer than those in the equatorial plane [i.e., Cu1–O4$^{\&}$ = 2.54(7) Å and Cu1–O4$^{\#}$ = 2.52(7) Å; symmetry codes: (&) $4-x$, $2-y$, $1-z$ and (#) $x-1$, $y-1, z$] resulting in the formation of tetragonally elongated octahedral structure. The geometry is commonly observed in the distorted octahedral coordination geometry of Cu(II) complexes and is explained by a Jahn–Teller effect [29].

One type of intramolecular hydrogen bond, N5–H5B···O4, stabilizes the conformation of the compound, while the crystal packing is stabilized by intermolecular hydrogen bonds N4–H4A···O5(DMF)^{i} and N5–H5A···O5(DMF)^{i}

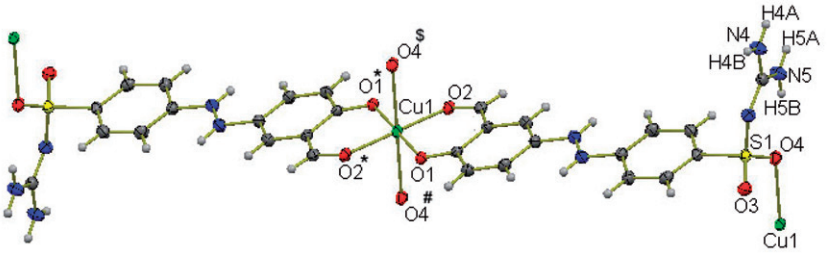

Figure 2. Molecular structure of **1** with 50% thermal ellipsoids [symmetry codes: (*) $-x+3, -y+1, -z+1$; ($) $4-x, 2-y, 1-z$; (#) $x-1, y-1, z$]; solvent molecules are omitted for clarity.

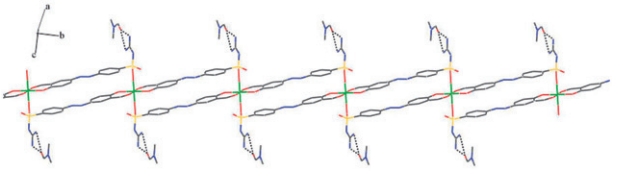

Figure 3. 1-D chain structure of **1** along the *b*-axis (solvent molecules involved in H-bonding are only shown).

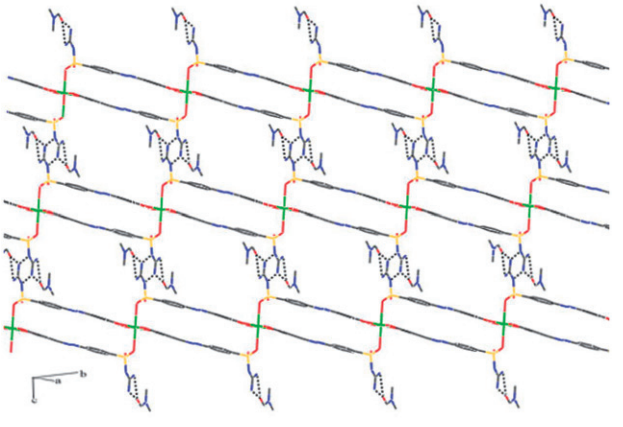

Figure 4. View of the 2-D hydrogen bonding framework of **2** extended along the *bc* plane (solvent molecules involved in H-bonding are only shown).

[symmetry code: (i) $3-x, 2-y, -z$]. A most effective intermolecular hydrogen bond is N4–H4B$\cdots$N3^{ii} [symmetry code: (ii) $4-x, 3-y, -z$], which links the 1-D polymeric chains together resulting in the formation of an extended 2-D layer parallel to the *bc* plane (figure 4).

3.6. *IR spectra*

Data of IR spectra of HL and the metal complexes are listed in table 5. Two bands that appear at 3453 and 3369 cm^{-1} in the ligand spectrum are attributed to asymmetric and

Table 5. IR data (4000–400 cm^{-1}) of HL and metal complexes.

No.	$\nu(NH_2)$	$\nu(C{=}O)$	$\nu(C{=}N)$	$\nu(SO_2)$	$\nu(C{-}O)$ Phen.	$\nu(M{-}O)$
HL	3453(m), 3369(s)	1651(m)	1630(s)	1375(m), 1132(s)	1205(w)	–
1	3428(s), 3319(s)	1662(sh)	1608(s)	1330(m), 1114(s)	1220(m)	516(w)
2	3390(s), 3312(s)	1660(sh)	1608(s)	1330(m), 1114(s)	1220(m)	516(w)
3	3434(w), 3343(w)	1633(sh)	1626(s)	1342(m), 1134(s)	1217(w)	542(w)
4	3449(m), 3395(m)	1640(w)	1626(s)	1338(w), 1112(m)	1219(w)	533(m)
5	3370(sh), 3326(w)	1614(s)	1626(sh)	1317(w), 1130(s)	1212(sh)	604(w)

s = strong, w = weak, sh = shoulder, m = medium, br = broad.

symmetrical vibrations of NH_2. The vibrations appear at higher or lower wavenumbers in spectra of the metal complexes, due to hydrogen bonds involving the amino groups. The band at 3483 cm^{-1} in the ligand spectrum corresponding to ν(OH) disappears in spectra of metal complexes, indicating coordination of the OH group to metal through deprotonation. This evidence is confirmed by shift of ν(C–O) in the ligand spectrum at 1205 cm^{-1} to higher wavenumbers in spectra of metal complexes [30]. The band at 1651 cm^{-1} in the ligand spectrum attributed to $\nu(C=O)$ appears in spectra of all metal complexes at higher or lower wavenumbers, confirming the coordination of C = O. The strong ligand band at 1630 cm^{-1}, assigned to $\nu(C=N)$, appears almost at the same position in spectra of **3**, **4**, and **5**. In **1** and **2**, the band is shifted to lower wavenumbers. The shift of the band may be due to the perturbing effect of coordination of SO_2 to the metal. Coordination of oxygen to the metal center is further supported by the appearance of non-ligand bands at 552–537 cm^{-1}, assigned to ν(M–O) [25].

3.7. *Electronic spectra and magnetic measurements*

UV-Vis spectra of the metal complexes were recorded in nujol mull from 200 to 800 nm. The six-coordinate Cu(II) complexes **1** and **2** display a broad absorption at 16,220 cm^{-1}, which can be assigned to $^2E_g \rightarrow {}^2T_{2g}$ transition reported for tetragonally distorted octahedral configuration [31]. The geometry of the Cu(II) complexes is further supported by the magnetic moment of 1.79 B.M. for **1** and **2**. The Co(II) complex **3** displayed three bands at 16,181, 21,231, and 25,275 cm^{-1} corresponding to $^4T_{1g}(F) \rightarrow {}^4A_{2g}(F)$, $^4T_{1g}(F) \rightarrow {}^4T_{1g}(P)$, and MLCT transitions, respectively, suggesting the possibility of an octahedral geometry [31]. The observed magnetic moment of **3** is 4.82 B.M., which can be taken as further support of octahedral geometry around the metal center. The electronic spectrum of the Mn(II) complex **4** displays two bands at 20,876 and 18,484 cm^{-1}, which can be assigned to $^6A_{1g} \rightarrow {}^4E_g(G)$ and $^6A_{1g} \rightarrow {}^4T_{1g}(4G)$ transitions in an octahedral geometry [32]. The observed magnetic moment of the complex is 5.96 B.M., which confirms the octahedral structure. The electronic spectra of the Pd(II) complex **5** displays three bands at 19,569, 16,920, and 14,880 cm^{-1} corresponding to $^1A_{1g} \rightarrow {}^1E_g$, $^1A_{1g} \rightarrow {}^1B_{1g}$, and $^1A_{1g} \rightarrow {}^1A_{2g}$ transitions, respectively, assigned to Pd(II) ions in a square-planar geometry [33]. This compound is diamagnetic as expected.

3.8. *ESR spectra*

ESR spectra of **1** and **2** and Mn(II) complex **4** were recorded at room temperature as polycrystalline samples. Complexes **1** and **2** showed identical ESR spectral patterns with $g_{\perp} = 2.12$ and $g_{||} = 2.05$. The trend $g_{\perp} > g_{||} > 2.0023$ indicates that the Cu center has d_z^2 ground state, characteristic for elongated tetragonal octahedral structures [34]. The g_{eff} value has a positive contribution from the value of the free electron (2.0023), which may be due to an increase in covalent nature between metal and ligand [35]. The G parameter determined as $G = g_{||} - 2/g_{\perp} - 2$, which is a measure of the exchange interaction between the metal centers in a solid sample of the complex, has also been calculated. According to Hathaway [36], if $G > 4$, the exchange interaction is negligible, but $G < 4$ indicates the considerable exchange interaction in the solid complexes. The G value for the complexes reported here is much less than 4, suggesting a considerable interaction in the solid state. The ESR spectra of the Mn(II) complex **4** showed a broad signal with g_{eff} value of 1.99, which reveals the existence of high-spin Mn(II) complex. The line broadening and the pattern of g-value reveals an octahedral geometry for this complex [37].

3.9. *XRD measurement*

Although crystallization and the X-ray structure determination of **3** and **4** have been unsuccessful so far, the powder diffractograms of the two compounds were in agreement with that simulated from the single-crystal structure of **2** and that measured for **1** (figure 5). These observations suggest that **1**, **3**, and **4** are isostructural with **2** [38, 39].

3.10. *Thermal analysis*

Thermal stability and thermal behavior of the metal complexes were studied by TGA and DTG techniques. The data including the stages of decomposition, temperature ranges, DTG peak temperatures, decomposition product loss, as well as found and the calculated mass loss percentages are listed in table 6; the TG/DTG thermograms of **4** are illustrated in figure 6. We selected **2** as representative example to study the thermal behavior. The TG thermogram of **2** shows three steps of decomposition within the temperature range 60–800°C. The first step appears within the range 60–166°C and involves the loss of non-coordinated DMF with a mass loss of 22.81% (calculated mass loss 22.47%). This step is accompanied by an endothermic DTG peak with maximum at 105°C. The organic ligand then decomposes in two successive steps which appear within the temperature ranges 166–306°C and 306–483°C, respectively, resulting in the formation of the thermally stable CuO as final product. These two steps are accompanied by two endothermic DTG peaks with maximum temperature at 249°C and 375°C, respectively. From table 6 it is clear that the thermal data confirm the suggested formulas based on elemental analyses.

3.11. *Cyclic voltammetry*

The main electrochemical data of HL, **1**, **2**, **3**, and **4** are given in table 7 and a representative voltammogram is shown in figure 7. The cyclic voltammogram of HL

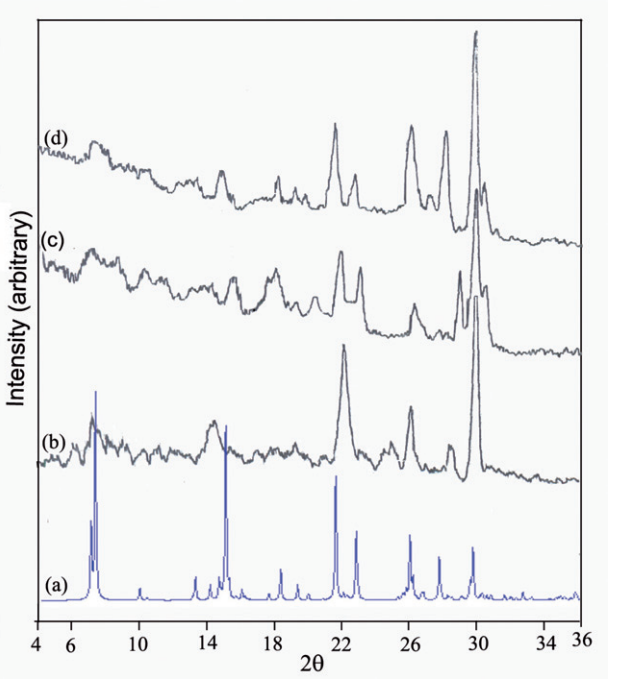

Figure 5. The XRD patterns of (a) **2** simulated from X-ray single-crystal data; (b) **1**; (c) **3**; (d) **4**.

Table 6. Thermoanalytical results of metal complexes.

Complex	TG range (°C)	DTG max (°C)	(Calcd) found mass loss (%)	Assignment	Metallic residue
1	236–347	304	(8.46) 8.85	–Loss of N_4H_8	CuO
	347–427	362	(20.09) 20.18	–Loss of $C_{12}H_8$	
	427–561	440	(61.12) 60.27	–Further decomposition of ligand	
2	60–166	105	(22.47) 22.81	–Loss of three DMF	CuO
	166–306	249	(37.72) 37.12	–Loss of $C_{24}H_{16}N_4O_4S_2$	
	306–483	375	(31.66) 31.46	–Further decomposition of ligand	
3	32–350	344	(15.43) 15.84	–Loss of $C_2H_8N_6$	CoO
	350–420	403	(64.92) 64.30	–Loss of $C_{24}H_{16}N_4O_4S_2$	
	420–558	494	(9.84) 10.52	–Further decomposition of ligand	
4	320–378	335	(8.56) 8.7	–Loss of N_4H_8	MnO
	378–494	406	(51.89) 52.33	–Loss of $C_{14}H_8N_6O_4S_2$	
	494–841	524	(30.26) 30.30	–Further decomposition of ligand	
5	29–130	90	(4.55) 4.32	–Loss of coord. H_2O	PdO
	130–230	188	(7.01) 7.12	–Loss of coord. Cl^-	
	230–408	315	(24.11) 24.98	–Loss of $CH_4N_3SO_2$	
	408–530	490	(40.23) 39.55	–Further decomposition of ligand	

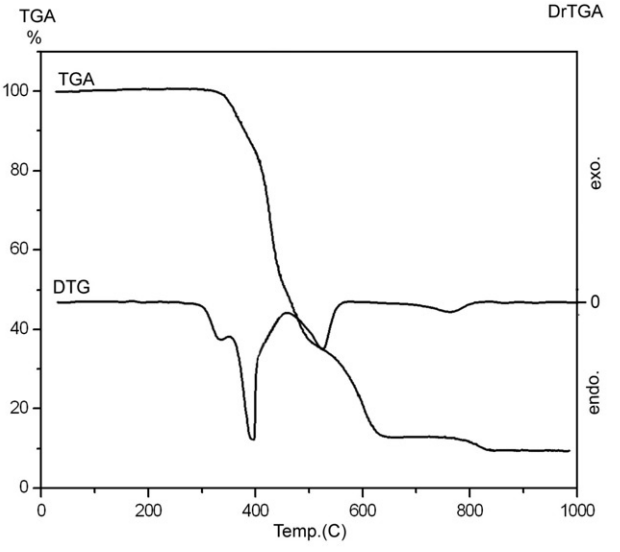

Figure 6. The TG and DTG curves of **4**.

Table 7. Electrochemical data for HL and its Cu(II), Co(II), and Mn(II) complexes.

	Cathodic side[a]				Anodic side		
Compound	$E_{pc}1$ (V)[b]	$E_{pc}2$ (V)	$E_{pa}1$ (V)[c]	$E_{pa}2$ (V)	$E_{pa}1$ (V)	$E_{pa}2$ (V)	$E_{pc}1$ (V)
HL	−1.42	–	–		0.66	–	–
1	−1.57	–	–		0.46		0.33
3	−1.49	−1.18	−1.32	−0.19	0.88	1.22	
4	−1.53	−1.17	−0.8		0.43	0.88	0.35

[a]Measurements were done in DMF solution at 100 mVs^{-1}; GC working electrode and Ag/AgCl reference electrode; TBAP supporting electrolyte (10^{-1} mol L^{-1}); compound concentration (10^{-3} mol L^{-1}).
[b]Cathodic peak potential.
[c]Anodic peak potential.

displays cathodic peak at $E_{pc} = -1.42$ V due to the reduction of azobenzene. The irreversible anodic peak which appears at $E_{pa} = 0.66$ V is assigned to oxidation of the azobenzene moiety [40].

The electrochemical behavior of **1** and **2** are identical. The cyclic voltammogram of **1** displays a ligand-based cathodic peak at $E_{pc} = -1.57$ V. The quasi-reversible process with $E_{pa} = 0.46$ V is assigned to Cu(II)/Cu(III) while the reduction peak located at $E_{pc} = 0.33$ V is assigned to the reverse process (i.e., Cu(III)/Cu(II)) [41]. The variation of the scan rate from 20 to 500 mVs^{-1} shows that the cathodic potential, E_{pc}, shifts to more negative value and ΔE_p also increases with increasing scan rate (figure 7), confirming the quasi-reversibility of the electrode process [41].

For **3**, two cathodic peaks at $E_{pc} = -1.49$ and -1.18 V and four anodic peaks at $E_{pa} = -1.32$, -0.19, 0.88, and 1.22 V are obtained. Quite similar behavior was observed by Ghames *et al.* [42] for octahedral Co(II) complex of a Schiff-base ligand.

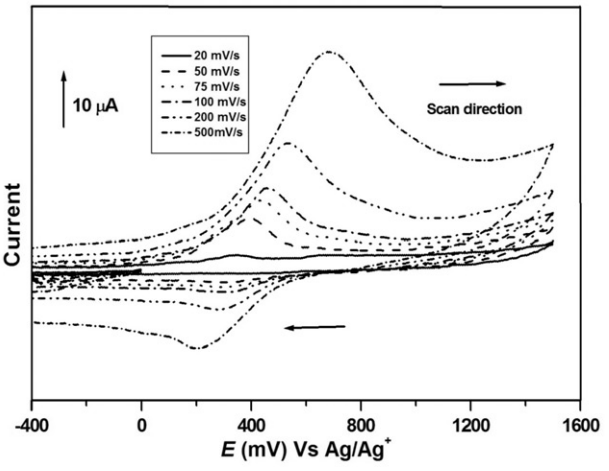

Figure 7. Cyclic voltammograms in DMF of **1** at successive scans.

The irreversible cathodic peak at −1.18 V is assigned to Co(II)/Co(I) while the anodic peak at −0.19 V corresponds to the reverse process (i.e., reoxidation of the reduced metal center).

For **4**, two cathodic peaks are observed at $E_{pc} = -1.53$ and −1.17 V and one anodic peak at $E_{pa} = -0.8$ V. The cathodic peak at −1.17 V can be assigned to Mn(II)/Mn(I) process while the anodic peak at −0.8 V can be assigned to the reverse process. In the anodic direction, two anodic peaks are observed at $E_{pa} = 0.43$ and 0.88 V and one cathodic peak at $E_{pc} = 0.35$ V. The anodic peak at 0.43 V can be assigned to Mn(II)/Mn(III) and reduction peak is located at $E_{pc} = 0.35$ V.

4. Conclusion

New polymeric Cu(II), Co(II), and Mn(II) complexes of sulfaguanidine azo dye (HL) in addition to the non-polymeric Pd(II) complex have been synthesized and characterized. The structures proposed are based on octahedral and tetragonally elongated octahedral geometry for Co(II), Mn(II), and Cu(II) complexes and a square-planar geometry for Pd(II) complex, in which the ligand serves as monobasic bidentate or tridentate. The conductance data revealed that the complexes are non-electrolytes. The thermal data confirmed the suggested formulas proposed based on elemental analyses (C, H, and N). Compounds **1**, **3**, and **4** were shown to be isomorphous to **2** by XRD. The crystal structures of HL and **2** were determined. The electrochemical behaviors of HL and its complexes were investigated using CV. The Cu(II) complexes **1** and **2** displayed a quasi-reversible wave with the anodic and cathodic peaks located at $E_{pa} = 0.46$ and $E_{pc} = 0.33$, respectively, which could be reasonably assigned as those corresponding to the Cu(II)/Cu(III) couple. For Co(II) complex, **3**, reduction of the metal center [Co(II)/Co(I)], appeared as an irreversible peak at −1.18 V and the anodic peak appearing at −0.19 V is assigned to the reverse process. Complex **4** displayed a cathodic peak at −1.17 V assigned to Mn(II)/Mn(I) and the anodic peak at 0.43 V is assigned to the

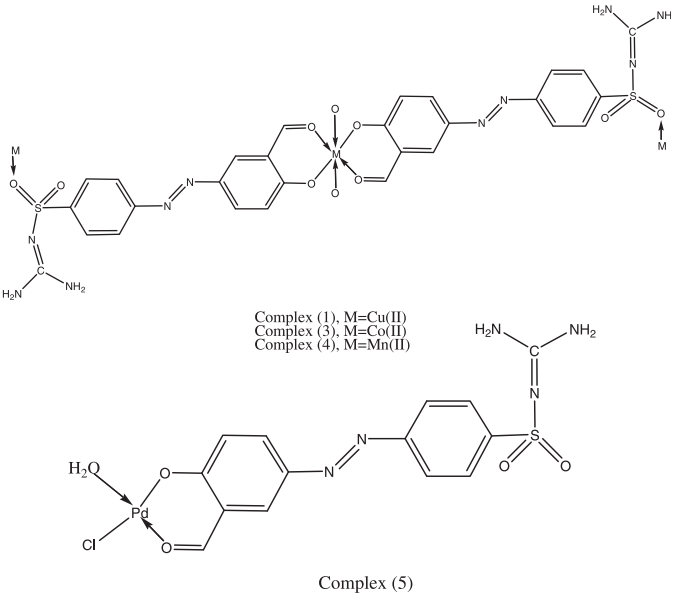

Scheme 2. Proposed structures for the metal complexes.

reverse process. Based on the analytical results, the proposed structures of the metal complexes are represented in scheme 2.

Supplementary material

CCDC 768589 and 768590 contain the supplementary crystallographic data for HL and **2**, respectively. These data can be obtained free of charge *via* http://www.ccdc.cam.ac.uk/conts/retrieving.html or from the Cambridge Crystallographic Data Centre, 12 Union Road, Cambridge CB2 1EZ, UK; Fax: (+44) 1223-336-033; or E-mail: deposit@ccdc.cam.ac.uk.

Acknowledgments

H. El-Ghamry acknowledges the Egyptian Channel System for the financial support to promote the joint research project between Tanta and Kyushu Universities. The authors also would like to thank Dr Kenji Yoza (Bruker AXS) for his help in the X-ray crystallographic analysis.

References

[1] J.M. Lehn. *Supramolecular Chemistry: Concepts and Perspectives*, VCH, Weinheim (1995).
[2] O. Ermer. *Adv. Mater.*, **3**, 608 (1991), and references therein.
[3] K. Inoue, T. Hayamizu, H. Iwamura, D. Hashizume, Y. Ohashi. *J. Am. Chem. Soc.*, **118**, 1803 (1996).
[4] T. Kitazawa, S. Nishikiori, R. Kuroda, T. Iwamoto. *J. Chem. Soc., Dalton Trans.*, 1029 (1994), and references cited therein.
[5] M. Albrecht, M. Lutz, A.L. Spek, G. Koten. *Nature*, **406**, 970 (2000).
[6] M. Fujita, Y.J. Kwon, S. Washizu, K. Ogura. *J. Am. Chem. Soc.*, **116**, 1151 (1994).
[7] S.W. Jin, W.Z. Chen. *Polyhedron*, **26**, 3074 (2007).
[8] P. Nagaraja, K. Sunith, R. Vasantha, H. Yathirajan. *Eur. J. Pharm. Biopharm.*, **53**, 187 (2002).
[9] A.Z. El-Sonbati, M.A. Diab, M.M. El-Halawany, N.E. Salam. *Spectrochim. Acta*, **75A**, 755 (2010), and references therein.
[10] A.Z. El-Sonbati, A.A. El-Bindary, R.M. Ahmed. *J. Solution Chem.*, **32**, 617 (2003).
[11] A.Z. El-Sonbati, A.A. El-Bindary, E.M. Mabrouk, R.M. Ahmed. *Spectrochim. Acta*, **57A**, 1751 (2001).
[12] A.Z. El-Sonbati, M.A. Diab, M.S. El-Shehawy, M. Moqbal. *Spectrochim. Acta*, **75A**, 394 (2010).
[13] P. Byabartta. *Dyes Pigm.*, **75**, 74 (2007).
[14] A.Z. El-Sonbati, M.A. Diab, M.M. El-Halawany, N.E. Salam. *Mater. Chem. Phys.*, **123**, 439 (2010).
[15] G.G. Mohamed, M.A. Gad-Elkareem. *Spectrochim. Acta*, **68A**, 1382 (2007).
[16] A.Z. El-Sonbati, R.M. Issa, A.M. Abd El-Gawad. *Spectrochim. Acta*, **68A**, 134 (2007).
[17] M. Mondelli, V. Brune, G. Borthagaray, J. Ellena, O.R. Nascimento, C.Q. Leite, A.A. Batista, M.H. Torre. *J. Inorg. Biochem.*, **102**, 285 (2008).
[18] A.T. Mubarak, A.Z. El-Sonbati, S.M. Ahmed. *J. Coord. Chem.*, **60**, 1877 (2007).
[19] *Mercury 1.4.2*, Copyright Cambridge Crystallographic Data Centre, 12 Union Road, Cambridge CB2 1EZ, UK (2001–2007).
[20] *Bruker APEX II*, Bruker AXS Inc., Madison, Wisconsin, USA (2006).
[21] G.M. Sheldrick. *SADABS*, University of Göttingen, Germany (1996).
[22] G.M. Sheldrick. *Acta Cryst.*, **64A**, 112 (2008).
[23] K. Sakai. *KENX*, Kyushu University, Japan (2004).
[24] M. Odabasoglu, C. Albayrak, R. Ozkanca, F. Aykan, P. Lonecke. *J. Mol. Struct.*, **840**, 71 (2007).
[25] C.M. Sharaby. *Spectrochim. Acta*, **62A**, 326 (2005).
[26] J. Geary. *Coord. Chem. Rev.*, **7**, 81 (1971).
[27] F.H. Allen, O. Kennard, D.G. Watson, L. Brammer, A.G. Open, R. Taylor. *J. Chem. Soc., Perkin Trans.*, **2**, S1 (1987).
[28] Z. Lin, W. Zeng. *Acta Cryst.*, **62E**, 1074 (2006).
[29] N. Okabe, E. Yamamoto, M. Yasunori. *Acta Cryst.*, **59E**, 715 (2003).
[30] R.C. Maurya, M.N. Jayaswal, R. Verma, B. Shukla. *Synth. React. Inorg. Met.-Org. Chem.*, **28**, 1265 (1996).
[31] H. Liu, H. Wang, F. Gao, D. Niu, Z. Lu. *J. Coord. Chem.*, **60**, 2671 (2007).
[32] R.M. Issa, S.A. Azim, A.M. Khedr, D.F. Draz. *J. Coord. Chem.*, **62**, 1859 (2009).
[33] A.B.P. Lever. *Inorganic Electronic Spectroscopy*, 2nd Edn, Elsevier, New York (1984).
[34] S.M. Abu-El-Wafa, N.A. El-Wakiel, R.M. Issa, R.A. Mansour. *J. Coord. Chem.*, **58**, 683 (2005).
[35] S.M. Abu-El-Wafa, R.M. Issa, C.A. McAuliffe. *Inorg. Chim. Acta*, **99**, 103 (1985).
[36] B.J. Hathaway, D.E. Billing. *Coord. Chem. Rev.*, **5**, 143 (1970).
[37] K.Y. El-Baredie. *Monatsh. Chem.*, **136**, 1139 (2005).
[38] J. Lefebvre, D. Chartrand, D.B. Leznoff. *Polyhedron*, **26**, 2189 (2007).
[39] A. Das, G. Pilet, D. Luneau, M.S. El Fallah, J. Ribas, S. Mitra. *Inorg. Chim. Acta*, **358**, 4581 (2005).
[40] M.M.M. Raposo, A.M.R. Sousa, A.M.C. Fonseca, G. Kirsch. *Tetrahedron*, **61**, 8249 (2005).
[41] N. Raman, A. Kulandaisamy, A. Shunmugasundaram. *Transition Met. Chem.*, **26**, 131 (2001).
[42] A. Ghames, T. Douadi, D. Haffar, S. Chafaa, M. Allain, M.A. Khan, G.M. Bouet. *Polyhedron*, **25**, 3201 (2006).